ALMA images of discs: are all gaps carved by planets?

J.-F. Gonzalez,[1]★ G. Laibe,[2] S. T. Maddison,[3] C. Pinte[4,5] and F. Ménard[4,5]

[1]*Université de Lyon, F-69003 Lyon, France; Observatoire de Lyon, Universite Lyon 1, 9 avenue Charles Andre, F-69230 Saint-Genis Laval, France; CNRS, UMR 5574, Centre de Recherche Astrophysique de Lyon; Ecole Normale Superieure de Lyon, F-69007 Lyon, France*

[2]*School of Physics and Astronomy, University of Saint Andrews, North Haugh, St Andrews, Fife KY16 9SS, UK*

[3]*Centre for Astrophysics and Supercomputing, Swinburne University of Technology, PO Box 218, Hawthorn, VIC 3122, Australia*

[4]*UMI-FCA, CNRS/INSU France (UMI 3386), and Departamento de Astronomía, Universidad de Chile, Casilla 36-D Santiago, Chile*

[5]*UJF-Grenoble 1/CNRS-INSU, Institut de Planétologie et d'Astrophysique de Grenoble, UMR 5274, Grenoble F-38041, France*

ABSTRACT

Protoplanetary discs are now routinely observed and exoplanets, after the numerous indirect discoveries, are starting to be directly imaged. To better understand the planet formation process, the next step is the detection of forming planets or of signposts of young planets still in their disc, such as gaps. A spectacular example is the Atacama Large Millimeter/submillimeter Array (ALMA) science verification image of HL Tau showing numerous gaps and rings in its disc. To study the observability of planet gaps, we ran 3D hydrodynamical simulations of a gas and dust disc containing a 5 M_J gap-opening planet and characterized the spatial distribution of migrating, growing and fragmenting dust grains. We then computed the corresponding synthetic images for ALMA. For a value of the dust fragmentation threshold of 15 m s^{-1} for the collisional velocity, we identify for the first time a self-induced dust pile-up in simulations taking fragmentation into account. This feature, in addition to the easily detected planet gap, causes a second apparent gap that could be mistaken for the signature of a second planet. It is therefore essential to be cautious in the interpretation of gap detections.

Key words: Methods: numerical – Planet-disc interactions – Protoplanetary discs – submillimetre: planetary systems.

1 INTRODUCTION

The holy grail in the field of planetary science is to catch planet formation in action, and the most anticipated signpost of massive planets in discs are gaps. Many gas-rich protoplanetary discs have now been observed with gaps and inner cavities, especially at sub-millimetre and millimetre wavelengths (e.g. Casassus et al. 2013; Canovas et al. 2015; van der Marel et al. 2015). These so-called transitional discs have inner regions which have undergone substantial clearing, due to a combination of grain growth, photoevaporation and/or interaction with an embedded planet or companion (Espaillat et al. 2014). While there are now a few examples of discs which show tantalizing evidence of embedded protoplanets and disc clearing (e.g. LkCa 15, Kraus & Ireland 2012; HD 100546, Quanz et al. 2015) direct observational evidence of planet clearing remains elusive. Planet gaps have been predicted theoretically for several decades (Papaloizou & Lin 1984) and many numerical studies of planets opening gaps have been conducted (e.g. Kley 1999; Paardekooper & Mellema 2004; Crida, Morbidelli & Masset 2006; de Val-Borro et al. 2006; Fouchet et al. 2007; Ayliffe et al. 2012), as

have predictions of their observability (Wolf et al. 2002; Gonzalez et al. 2012; Ruge et al. 2013).

More recently, the spectacular Atacama Large Millimeter/submillimeter Array (ALMA) science verification images of HL Tau (ALMA Partnership et al. 2015) surprised everyone with its clearly discerned multiple rings and gaps, which even more surprisingly are axisymmetric. It is tempting to attribute each ring plus gap in the ALMA image of HL Tau to a planet, but is this the right thing to do? Zhang, Blake & Bergin (2015) invoke potential accumulation of dust at condensation fronts. However, the location of the first three gaps observed by ALMA in HL Tau are found to be close to mean motion resonances, suggesting that the rings could be generated by planets (ALMA Partnership et al. 2015). The question we address in this Letter is whether all gaps seen in protoplanetary discs are always planet gaps, or could they result from alternative processes occurring during the early stages of planet formation? We explore here the effects of dust pile-up as such an alternative.

Millimetre continuum images trace the spatial distribution of dust grains. Their evolution in discs is governed by two parameters. The first is the Stokes number, St, which is the ratio of the drag stopping time to the orbital period. The value of St determines the efficiency of vertical settling, radial drift and growth/fragmentation of grains in

★ E-mail: Jean-Francois.Gonzalez@ens-lyon.fr

the disc (e.g. Weidenschilling 1977; Nakagawa, Sekiya & Hayashi 1986; Stepinski & Valageas 1997; Youdin & Shu 2002; Garaud & Lin 2004; Haghighipour 2005; Brauer, Dullemond & Henning 2008; Birnstiel, Dullemond & Brauer 2010; Laibe 2014). In particular, grain migration is fastest when St $\sim$ 1. St is a function of the grain size and density, but depends also on the local gas conditions. As such, it varies as a function of the distance to the central star for a given grain size. HL Tau is a young and massive extended disc supplied by in-falling material from the surrounding envelope. For such discs, millimetre-sized grains have St $\sim$ 1 at a few tens of au, at which point the dust and gas strongly decouple (Laibe, Gonzalez & Maddison 2012). The second parameter involved is the dust-to-gas ratio ϵ. For ϵ of order unity, dust affects the gas as much as gas affects dust due to aerodynamic drag. Although the dust backreaction due to dust inertia is negligible in most astrophysical systems, it becomes critical in regions of discs where dust concentrates, such as particles traps.

In this Letter, we present a mechanism where grain growth and fragmentation result in dust distributions that produce apparent gaps when the dust backreaction is taken into consideration. We provide the details on our numerical simulations and synthetic observables in Section 2, discuss the origin of the apparent gap in Section 3, and conclude in Section 4.

2 METHODS AND RESULTS

2.1 Hydrodynamic simulations

We study the evolution of gas and dust in protoplanetary discs using our 3D, two-phase, smoothed particle hydrodynamics (SPH) code, described in Barrière-Fouchet et al. (2005). We self-consistently treat the aerodynamical drag between gas and dust, including the backreaction of dust on gas. We follow the standard SPH implementation of artificial viscosity (Monaghan 1989) and use $\alpha_{SPH} = 0.1$ and $\beta_{SPH} = 0.5$, corresponding to a uniform Shakura & Sunyaev (1973) parameter $\alpha_{SS} \sim 10^{-2}$ (see Fouchet et al. 2007, for a discussion). Arena & Gonzalez (2013) showed that the expected properties of turbulence are naturally reproduced by the SPH formalism. Grain growth is treated as described in Laibe et al. (2008), via the prescription developed by Stepinski & Valageas (1997) based on the determination of the relative velocity of grains, $V_{rel} \propto c_s \sqrt{\alpha_{SS} St}/(1 + St)$, as a function of local properties of the gas phase (e.g. its sound speed c_s) and grain size. We implement grain fragmentation by defining a velocity threshold, V_{frag}, to which we compare V_{rel}. Collisions occurring at speeds below the thresh-

old velocity lead to grain growth, while collisions at greater speeds result in the shattering of grains, which we model by decreasing the size of the representative grains. The numerical procedure is detailed in Gonzalez et al. (2015).

We model a disc typical of Classical T Tauri Stars (CTTS) of mass $M_{disc} = 0.01\,M_{\odot}$ around a 1 $M_{\odot}$ star, with an initially uniform dust-to-gas ratio $\epsilon = 10^{-2}$. The disc contains a 5 M_J planet on a circular orbit at a fixed radius of $r_p = 40$ au. The planet is implemented as a point mass particle subject only to the star's gravity, whereas the SPH gas and dust particles feel the gravitational potential of the star and planet (see Fouchet et al. 2007). The disc is initially set up as in Fouchet, Gonzalez & Maddison (2010) with a constant surface density $\Sigma(r) = 19.67$ kg m^{-2} with radial extension from 4 to 120 au, a vertically isothermal temperature profile $T(r) = 15\,(r/r_p)^{-1}$ K, and is free to evolve. Grains have an initially uniform size $s_0 = 10\,\mu$m and are allowed to grow and fragment. In Gonzalez et al. (2015), we presented a suite of simulations that vary the fragmentation threshold: $V_{frag} = 10, 15, 20, 25$ m s^{-1} and $+\infty$ (i.e. growth only), evolved for 100 000 yr or $\sim$400 planetary orbits, and discussed our choice of parameters and their influence on the results. In particular, our disc temperature is colder than what observations suggest (e.g. Williams & Best 2014). Changing its value would affect gap formation (only moderately for a high-mass planet), as well as fragmentation ($V_{rel} \propto c_s \propto \sqrt{T}$). In the mid-plane, St is independent of T, leaving dust dynamics unchanged. In this Letter, we focus on the $V_{frag} = 15$ m s^{-1} case, for which we see a second apparent gap.

Fig. 1 shows the gas and dust volume densities ρ_g and ρ_d, as well as the grain size s in the disc mid-plane at the end of the simulation. The planet at 40 au has opened a gap in the gas phase and much of the disc interior to the gap has been accreted on to the star, leaving a central low-density area. In the dust phase, the gap is more prominent, with sharper edges. Some material remains in the inner disc and grains have accumulated at the dust trap located at the gap outer edge. These properties are commonly seen in studies of planet gaps in gas+dust discs (see e.g. Paardekooper & Mellema 2004; Fouchet et al. 2010). An unexpected feature is the second high-density ring in the dust disc at $r \sim 90$ au visible in the density map (centre panel of Fig. 1) and in the radial profile of the mid-plane volume density (Fig. 2). Large grains (mm to cm in size) are abundant in the high-density regions (right-hand panel of Fig. 1 and bottom panel of Fig. 2), where relative velocities between grains are lowest and grain growth is more efficient. The dust population is best characterized in Fig. 3, showing the distribution of grains in the meridian plane and their radial size
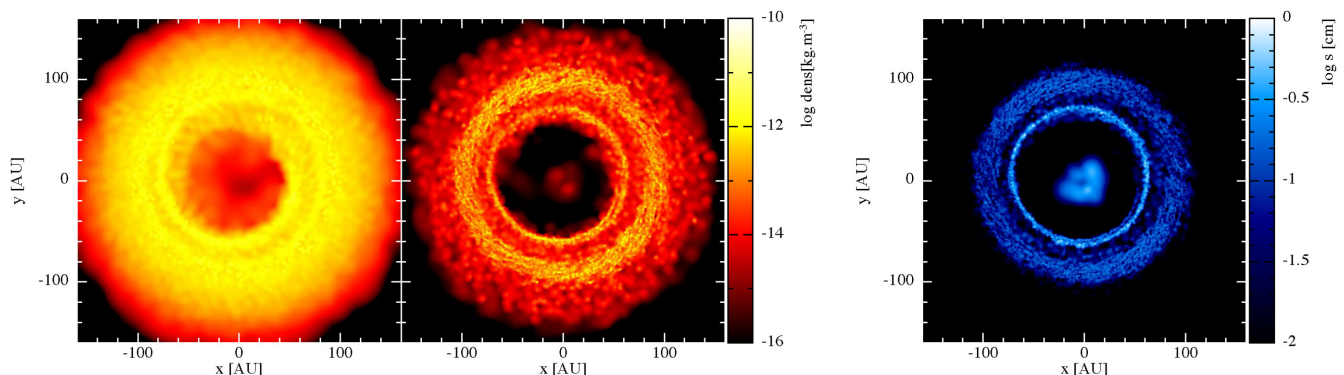

Figure 1. Maps of the volume density of the gas (left) and dust (centre) and of the average dust grain size (computed with the SPH kernel, right) in the disc mid-plane after 100 000 yr.
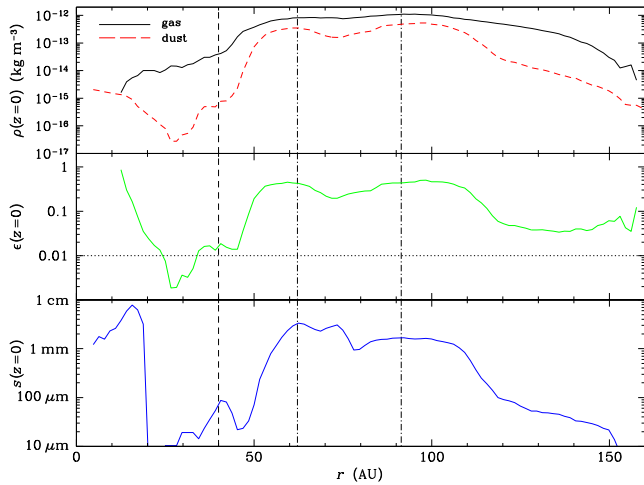
Figure 2. Azimuthally averaged radial profiles of the gas and dust volume densities (top), dust-to-gas ratio (middle), and mean grain size (bottom) in the mid-plane after 100 000 yr. The vertical dashed line shows the planet orbital radius, the vertical dash–dotted lines show the locations of pressure maxima (see Fig. 6) and the horizontal dotted line shows the initial dust-to-gas ratio.
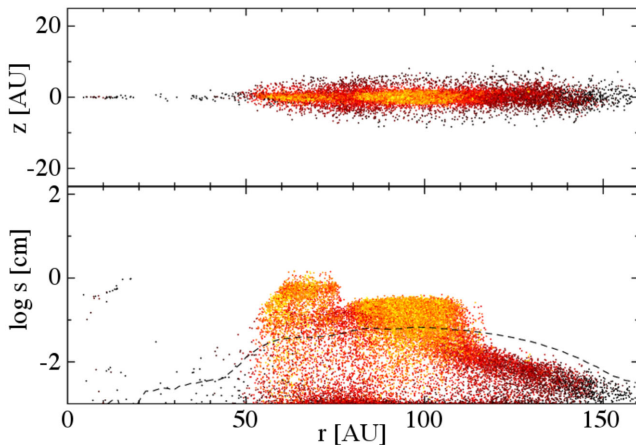

Figure 3. Meridian plane cut of the dust distribution (top) and radial grain size distribution (bottom) after 100 000 yr. The colour represents the volume density and is the same as in Fig. 1. The dashed line marks the grain size for which St = 1 in the disc mid-plane (see Section 3).

distribution. Two populations can be distinguished: grains that have been trapped in a narrow ring at the outer planet gap edge (at $r \sim 60$ au) and have grown, and grains that have started to grow in the outer disc, migrated inwards, decoupled from the gas, and piled up in a wider ring ~ 90 au from the star. We refer the reader to Gonzalez et al. (2015) for a detailed discussion of dust evolution, as well as Section 3.

2.2 Synthetic ALMA images

We produced synthetic ALMA images for the final state of our disc. We first computed raw intensity maps from the resulting dust distribution using the 3D Monte Carlo continuum radiative transfer code MCFOST (Pinte et al. 2006, 2009). It computes the scattering, absorption and re-emission of photons by dust grains assumed to be homogeneous spheres and composed of astronomical silicates, with optical properties derived according to Mie theory. These maps were
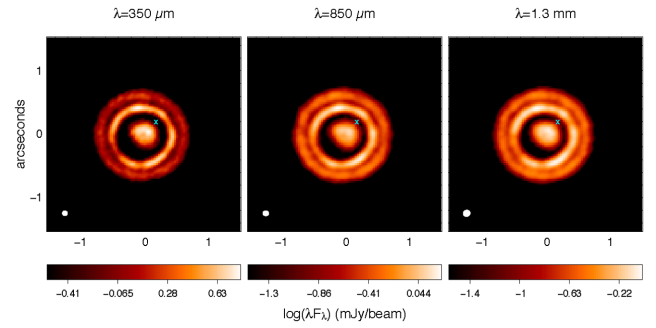
Figure 4. Simulated ALMA observations of a disc viewed nearly face-on at $d = 140$ pc and $\delta = -23°$ for an integration time of 1 h and angular resolution of 0.1 arcsec. From left to right: $\lambda = 350$ µm, 850 µm, and 1.3 mm. The scale on each image is in arcsec, with the beam size represented at its bottom-left corner, and the colour bar gives the flux in mJy beam^{-1}. The planet's position is marked with a cross.
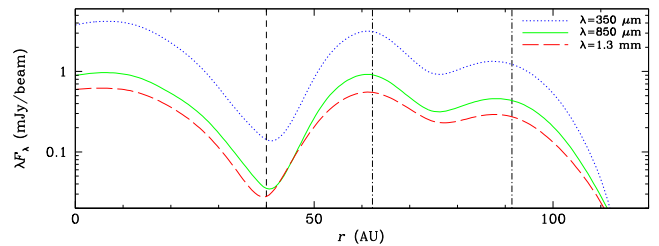

Figure 5. Radial cut of the brightness profile in the ALMA synthetic images for $\lambda = 350$ µm, 850 µm, and 1.3 mm. The vertical dashed line shows the planet orbital radius and the vertical dash–dotted lines show the locations of pressure maxima (see Fig. 6).

then passed to the CASA simulator for ALMA to obtain synthetic images for a given observing configuration (wavelength, angular resolution, integration time). For more details about this procedure, see Gonzalez et al. (2012).

Fig. 4 shows the resulting synthetic images at three different wavelengths: 350 µm, 850 µm, and 1.3 mm. They were computed for a nearly face-on orientation, a distance $d = 140$ pc and a declination $\delta = -23°$ (for which the source passes through the zenith at the ALMA site), an integration time $t = 1$ h and angular resolution $\theta = 0.1$ arcsec (found to be optimal observing parameters for gap detection by Gonzalez et al. 2012). We also plot in Fig. 5 radial cuts of the brightness profile for the three wavelengths. All images show the central emission from the dust in the inner disc (interior to 20 au, see Fig. 1), the deep and wide planet gap (centred on 40 au), a bright ring corresponding to the outer edge of the planet gap (near 60 au), a second shallower and narrower apparent gap (centred on ∼75 au, which happens to be near the 2:5 resonance with the planet), and finally a second fainter ring (centred on ∼90 au). The synthetic observations thus recover all features of the dust distribution. Note that a higher disc temperature would increase the computed fluxes, but would preserve the gap structures (see Section 2.1 for the influence of T on the dynamics).

3 DISCUSSION

We find that, in a CTTS disc containing a 5 M_J planet on a fixed circular 40 au orbit, a fragmentation threshold of $V_{frag} = 15$ m s^{-1} produces two almost axisymmetric gap and ring pairs in the corresponding synthetic images at (sub)millimetre wavelengths (Fig. 4). What is their origin? Lower continuum emission at a given location
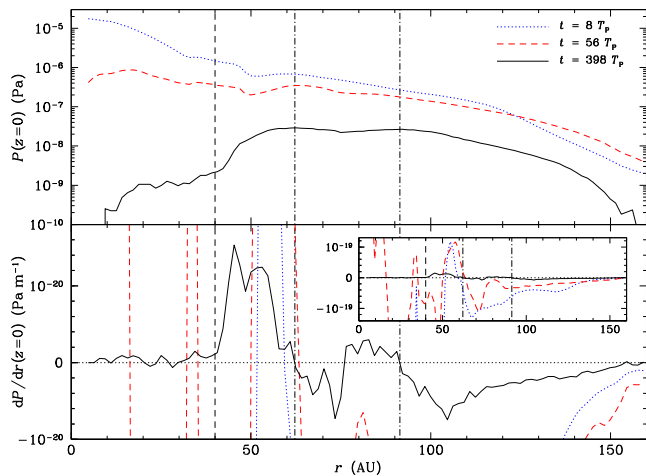
Figure 6. Azimuthally averaged profiles of the gas pressure (top) and pressure gradient (bottom) in the mid-plane after 8, 56, and 398 planet orbits (∼2000, 14 000, and 100 000 yr). The vertical dashed line shows the planet orbital radius and the vertical dash–dotted lines show the locations of pressure maxima at the end of the simulation. The inset shows a larger vertical scale.

corresponds to lower dust opacity at millimetre wavelengths, which can be caused by a local minimum of the dust density or by grain sizes outside of the range contributing significantly at these wavelengths (i.e. 100 μm to a few mm, for the dust optical properties assumed here), or both. It is important to note that the two gaps in our disc have different origins.

The planet is massive enough to carve a gap in the gas phase and produce a local pressure maximum at the outer gap edge ($r \sim 60$ au) very early in the disc evolution – see the mid-plane pressure and pressure gradient profiles in Fig. 6. Dust particles are trapped at the pressure maximum, accumulate, and grow more efficiently as they concentrate. This so-called particle trap generates the first ring just outside the planet gap (see also Pinilla, Benisty & Birnstiel 2012).

The second ring, on the other hand, is caused by a grain pile-up rather than a trap due to the planet. Grains can grow when V_{rel} (which scales as $c_s \propto r^{-1/2}$ in our disc) is small enough to stay below V_{frag}, i.e. in the disc outer regions. The growth time-scale varies as $r^{3/2}$ (Laibe et al. 2008), it is thus shorter at the inner boundary of this growth region. Growing grains migrate inwards, more rapidly as their size approaches the value for which St = 1 (plotted as a dashed line in Fig. 3 at the end of the simulation, see Gonzalez et al. 2015 for the time evolution). As grains continue to grow, they overcome the St = 1 regime, causing them to decouple from the gas, which slows their radial migration and results in a pile-up near 90 au. This enhances the local concentration of grains, and the dust-to-gas ratio approaches unity (see the middle panel of Fig. 2), which (i) stops grain migration in the accumulation region (Nakagawa et al. 1986) and (ii) starts to modify the gas density profile due to the backreaction of dust on gas. Indeed, the drag force between gas and dust is symmetric and in a dust concentration, it is gas that is dragged by the dust. This effect can only be seen in self-consistent simulations of the simultaneous evolution of gas and dust taking backreaction into account. In other words, the complex interplay between growth and migration induces dust self-accumulation, which causes the gas to accumulate at the dust concentration and form a second gas pressure maximum around $r \sim 90$ au at late times (see Fig. 6). This effectively results in a second particle trap, causing the second ring. This mechanism, predicted theoretically by Laibe (2014), is inde-

pendent of the presence of a planet, and was also seen in the very inner disc for the growth-only simulations in Gonzalez et al. (2015). Here, we identify for the first time a self-induced dust pile-up in simulations taking fragmentation into account.

Counter-intuitively, the value of the fragmentation threshold plays an essential role in the generation of this second ring. The dust pile-up occurs near the location where St = 1 for the largest grains, for which V_{rel} is also equal to V_{frag}, i.e. where $c_s \sqrt{\alpha_{SS}} \sim V_{frag}$. For a sound speed given by $c_s = c_{s,0}(r/r_0)^{-q/2}$, this location is approximated by $r_{pu}/r_0 \sim (\alpha_{SS} c_{s,0}^2/V_{frag}^2)^{1/q}$. In our disc and for $V_{frag} = 15$ m s^{-1}, $r_{pu} \sim 90$ au. For larger values of V_{frag}, grains would pile up at smaller orbital distances (∼50 and ∼30 au for $V_{frag} = 20$ and 25 m s^{-1}) but they are trapped at the planet gap outer edge before they can decouple. There is only one ring in this case. On the other hand, for smaller V_{frag}, only grains at very large orbital distances can grow, but because of their even lower growth rate they do not reach St = 1 and do not decouple before the end of the simulation (see Gonzalez et al. 2015, for illustrations of both cases). V_{frag} ranges from 1 to 10 m s^{-1} for compact silicate and icy grains (Blum & Wurm 2008) to several tens of m s^{-1} for porous aggregates (Yamamoto, Kadono & Wada 2014). The value of 15 m s^{-1}, producing a second ring that is well separated from the outer gap edge, would match moderately porous ice. However, different values of V_{frag}, or similarly of α_{SS} or the disc temperature, can still lead to two separate rings if the planet location is changed.

The second apparent gap is therefore the region of lower dust density between both dust accumulations. Its properties differ from those of a planet gap: the decrease in the density of both gas and dust is modest and the grains have grown to moderate sizes. However, the observational signatures of both the planet gap and the apparent gap are very similar, both in the images (Fig. 4) and in the brightness profiles (Fig. 5), so that the shallower apparent gap seems to mimic a gap that would be carved by a lighter planet orbiting at ∼75 au (all the more so that it would lie close to the 2:5 resonance with the planet at 40 au). Measuring this gap's width would give an estimate of this hypothetical planet's mass (Crida et al. 2006), but would not unambiguously prove its existence. Cuello (in preparation) ran a series of simulations with two planets embedded in the same disc as ours. With planets of 5 M_J at 40 au and 1 M_J at 80 au, the outer planet gap has a similar depth in the gas as our apparent gap (also in agreement with Kanagawa et al. 2015) but a much deeper gap in the dust. Conversely, a lighter outer planet would be needed to reproduce the depth of our apparent gap in the dust, but it would carve an even shallower gap in the gas. If a suitable tracer of gas in the gap can be found, ALMA observations of both gas and dust and the comparison of gap depth in both phases would thus be able to distinguish an apparent gap from a planet gap.

4 CONCLUSION

We have presented 3D hydrodynamical simulations of the evolution of gas and dust in a CTTS disc containing a planet which carves a gap in the disc. We self-consistently treat the interaction of gas and dust via aerodynamic drag and include grain growth and fragmentation. We then computed synthetic ALMA images from the resulting disc structure. We have shown that when the fragmentation threshold $V_{frag} = 15$ m s^{-1}, the dust dynamics results in the first documented self-induced pile-up of grains when fragmentation is included, at large distances from the star. This forms a dense dust ring containing mm-sized grains in the outer disc, away from the planet gap and the dust trap at its outer edge. In the images, in addition to the gap+ring

pair corresponding to the planet gap and its dense outer edge, this feature produces a second ring separated from the outer gap edge by an apparent gap, effectively resulting in a second gap+ring pair. This second, exterior gap does not contain a planet.

The recent spectacular ALMA image of the HL Tau disc (ALMA Partnership et al. 2015) shows as many as seven gap and ring pairs. Is each of them an actual planet gap? The answer is probably no and we have shown here one example for which it is not the case. More gaps in discs are likely to be detected as ALMA is ramping up to full operation and they will have to be interpreted with care. Comparison of gap depths in both gas and dust would help to distinguish a planet gap from an apparent gap such as presented here.

ACKNOWLEDGEMENTS

REFERENCES

ALMA Partnership et al., 2015, ApJ, 808, L3
Arena S. E., Gonzalez J.-F., 2013, MNRAS, 433, 98
Ayliffe B. A., Laibe G., Price D. J., Bate M. R., 2012, MNRAS, 423, 1450
Barrière-Fouchet L., Gonzalez J.-F., Murray J. R., Humble R. J., Maddison S. T., 2005, A&A, 443, 185
Birnstiel T., Dullemond C. P., Brauer F., 2010, A&A, 513, A79
Blum J., Wurm G., 2008, ARA&A, 46, 21
Brauer F., Dullemond C. P., Henning T., 2008, A&A, 480, 859
Canovas H. et al., 2015, ApJ, 805, 21
Casassus S. et al., 2013, Nature, 493, 191
Crida A., Morbidelli A., Masset F., 2006, Icarus, 181, 587
de Val-Borro M. et al., 2006, MNRAS, 370, 529
Espaillat C. et al., 2014, in Beuther H., Klessen R. S., Dullemond C. P., Henning T., eds, Protostars and Planets VI. Univ. Arizona Press, Tucson, AZ, p. 497
Fouchet L., Maddison S. T., Gonzalez J.-F., Murray J. R., 2007, A&A, 474, 1037
Fouchet L., Gonzalez J.-F., Maddison S. T., 2010, A&A, 518, A16
Garaud P., Lin D. N. C., 2004, ApJ, 608, 1050
Gonzalez J.-F., Pinte C., Maddison S. T., Ménard F., Fouchet L., 2012, A&A, 547, A58
Gonzalez J.-F., Laibe G., Maddison S. T., Pinte C., Ménard F., 2015, Planetary & Space Science, preprint (arXiv:1506.00430)
Haghighipour N., 2005, MNRAS, 362, 1015
Kanagawa K. D., Muto T., Tanaka H., Tanigawa T., Takeuchi T., Tsukagoshi T., Momose M., 2015, ApJ, 806, L15
Kley W., 1999, MNRAS, 303, 696
Kraus A. L., Ireland M. J., 2012, ApJ, 745, 5
Laibe G., 2014, MNRAS, 437, 3037
Laibe G., Gonzalez J.-F., Fouchet L., Maddison S. T., 2008, A&A, 487, 265
Laibe G., Gonzalez J.-F., Maddison S. T., 2012, A&A, 537, A61
Monaghan J. J., 1989, J. Comput. Phys., 82, 1
Nakagawa Y., Sekiya M., Hayashi C., 1986, Icarus, 67, 375
Paardekooper S.-J., Mellema G., 2004, A&A, 425, L9
Papaloizou J., Lin D. N. C., 1984, ApJ, 285, 818
Pinilla P., Benisty M., Birnstiel T., 2012, A&A, 545, A81
Pinte C., Ménard F., Duchêne G., Bastien P., 2006, A&A, 459, 797
Pinte C., Harries T. J., Min M., Watson A. M., Dullemond C. P., Woitke P., Ménard F., Durán-Rojas M. C., 2009, A&A, 498, 967
Price D. J., 2007, PASA, 24, 159
Quanz S. P., Amara A., Meyer M. R., Girard J. H., Kenworthy M. A., Kasper M., 2015, ApJ, 807, 64
Ruge J. P., Wolf S., Uribe A. L., Klahr H. H., 2013, A&A, 549, A97
Shakura N. I., Sunyaev R. A., 1973, A&A, 24, 337
Stepinski T. F., Valageas P., 1997, A&A, 319, 1007
van der Marel N., van Dishoeck E. F., Bruderer S., Pérez L., Isella A., 2015, A&A, 579, A106
Weidenschilling S. J., 1977, MNRAS, 180, 57
Williams J. P., Best W. M. J., 2014, ApJ, 788, 59
Wolf S., Gueth F., Henning T., Kley W., 2002, ApJ, 566, L97
Yamamoto T., Kadono T., Wada K., 2014, ApJ, 783, L36
Youdin A. N., Shu F. H., 2002, ApJ, 580, 494
Zhang K., Blake G. A., Bergin E. A., 2015, ApJ, 806, L7

This paper has been typeset from a TeX/LaTeX file prepared by the author.